Division of Engineering Research On-Call Services

Task 2: Rating of the Stringer System of the Approach Spans of the Combs-Hehl Bridge

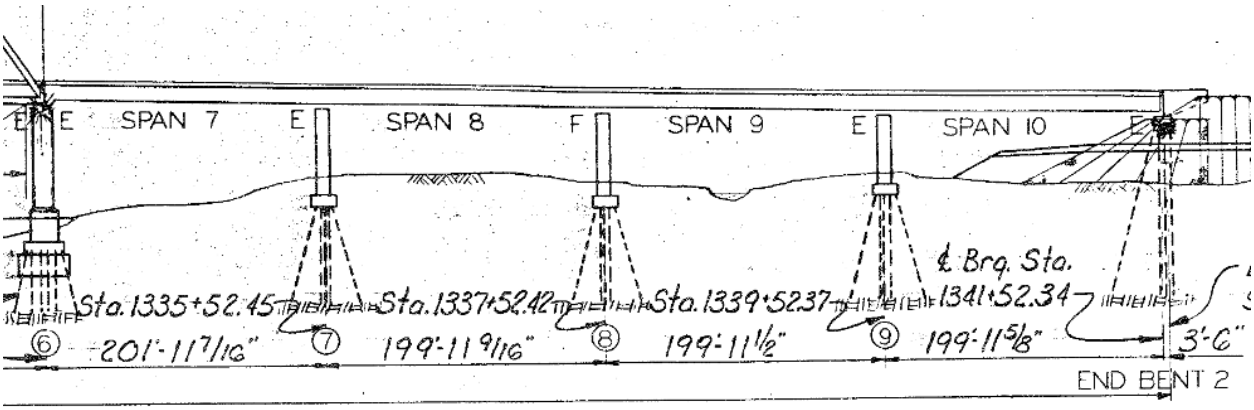

Prepared by:
James A Swanson
Gian Andrea Rassati
Rachel A Chicchi
Martin A Butler

Prepared for:
The Ohio Department of Transportation,
Office of Statewide Planning & Research

State Job Number #135785

June 2019

Final Report

U.S. Department of Transportation
Federal Highway Administration

Technical Report Documentation Page

1. Report No.	2. Government Accession No.	3. Recipient's Catalog No.
FHWA/OH-2019-15		

4. Title and Subtitle	5. Report Date
Division of Engineering Research On-Call Services **Task 2: Rating of the Stringer System of the Approach Spans of the Combs-Hehl Bridge**	**June 2019** 6. Performing Organization Code

7. Author(s)	8. Performing Organization Report No.
James A Swanson, Gian Andrea Rassati, Rachel A Chicchi, and Martin A Butler	

9. Performing Organization Name and Address	10. Work Unit No. (TRAIS)
Dept Civil and Architectural Engineering and Construction Management, University of Cincinnati, Cincinnati, OH 45221-0071	11. Contract or Grant No. **SJN 135785**

12. Sponsoring Agency Name and Address	13. Type of Report and Period Covered
Ohio Department of Transportation **1980 West Broad Street** **Columbus, Ohio 43223**	**Final Report for Task #2 of ROC** 14. Sponsoring Agency Code

15. Supplementary Notes

16. Abstract

17. Keywords	18. Distribution Statement
	No restrictions. This document is available to the public through the National Technical Information Service, Springfield, Virginia 22161

19. Security Classification (of this report)	20. Security Classification (of this page)	21. No. of Pages	22. Price
Unclassified	**Unclassified**		

Form DOT F 1700.7 (8-72) **Reproduction of completed pages authorized**

Division of Engineering Research On-Call Services

Task 2: Rating of the Stringer System of the Approach Spans of the Combs-Hehl Bridge

Prepared by:
James A Swanson
Gian Andrea Rassati
Rachel A Chicchi
Martin A Butler

Dept. of Civil and Architectural Engineering
and Construction Management
College of Engineering and Applied Science
University of Cincinnati

June 2019

Prepared in cooperation with the Ohio Department of Transportation
and the U.S. Department of Transportation, Federal Highway Administration

Acknowledgments

Advice at the beginning of the project from Victor J Hunt and Arthur J Helmicki at the University of Cincinnati is gratefully acknowledged, as is the support of the technical advisory panel throughout the project.

Overview

The Combs-Hehl Bridge is a series of structures over the Ohio River near Cincinnati spanning between Ohio on the east end and Kentucky on the west end. The overall bridge consists of four approach spans on the Kentucky side of the river (spans 1-4), two main truss spans over the river, (spans 5 and 6), and four approach spans on the Ohio side of the river (spans 7-10). The bridge carries interstate route 275 and, as a result, consists of two independent structures: the north bridge carrying westbound traffic and the south bridge carrying eastbound traffic. The scope of work for the project described herein was limited to rating of the stringers in the Ohio approach spans of the north and south bridges, identified as spans 7-10.

The Ohio approach spans of the south bridge consist of five stringers spaced at 8'-2½" spanning 25'-0" between floor beams that are supported by two girders. These girders are spaced at 32'-10" and are supported by piers spaced at 200', for an overall length of 800'. Because of an on-ramp for the westbound traffic on the Ohio side of the river, the north bridge is similar, but not identical, to the south bridge. The Ohio approach spans of the north bridge consist of seven stringers spanning 25'-0" between floor beams that are supported by two girders. The north bridge girders are also supported by piers spaced at 200', for an overall length of 800'. Since the north bridge was designed to accommodate an on ramp, the width of the bridge changes over its length, with stringer spacing varying from 5'-5½" to 8'-3" and the girder spacing varying from 32'-9" to 49'-6".

The analysis and rating of the approach spans were conducted using three methods. The first method was based on one-dimensional beam-line (1DBL) models to determine demands and traditional hand calculations to determine capacity. The second approach was based on three-dimensional linear and elastic (3DLE) finite element analyses of the bridges to determine demands and traditional hand calculations to determine capacity. The third approach was based on three-dimensional nonlinear and inelastic (3DNI) finite element analyses of the bridges wherein the finite element model itself was able to determine both the demand on, and the capacity of, the stringers. Each of the methods is described in the subsequent sections.

The ratings based on 1DBL analyses were automated and provided relatively conservative results for many truckloads in many different positions on the bridges. Ratings based on the 3DLE analyses were more rigorous and provided less conservative results than the 1DBL analyses but were used to investigate only truckloads and positions that were found to be most critical from the 1DBL analyses. Ratings based on the 3DNI analyses were the least conservative and were used to evaluate the strength of the bridges under the most critical truckloads and positions as determined from the 1DBL and 3DLE analyses and ratings.

In each of the rating methods, only the strong-axis moment strength of the stringers was considered. Additional elements such as floor beams, girders, splices, connections, and the deck were not evaluated for strength. One exception to this is that web buckling and web yielding strength checks of the stringers were conducted at the request of the ODOT advisory panel. Stringers were not evaluated for shear strength, fatigue, axial force, or the possibility of combined

axial force and moment. It should be noted that lateral and axial loading could reduce lateral-torsional buckling strength of the stringers. It was also assumed that the deck provides continuous lateral support to the top flanges of the stringers.

1D Beam-Line Modeling

The first method that was used to analyze and rate the stringers was based on a one-dimensional beam-line model. The SAP2000 finite element package was used to generate influence lines for a representative stringer supported by vertically rigid pins and rollers at 25'-0" intervals that represented the locations of the floor beams in the bridges. Stringer J, the center stringer in the south bridge, consisting of W24×76 and W24×55 sections, was selected as representative. Influence lines for strong axis moment were extracted at 10^{th} points and quarter points of each 25'-0" long stringer span over the full 800' length of the approach spans. The influence lines were generated by placing a unit vertical point load at 6" intervals over the full 800' length of the approach spans.

Permanent loads were determined and applied to the influence lines. Permanent loads were distributed evenly to the five stringers and two girders in the south bridge, and to the seven stringers and two girders in the north bridge. Both maximum and minimum load factors were considered for permanent loads; maximum load factors were applied when permanent loads were additive to the effects of truckloads and minimum load factors were applied when permanent loads mitigated the effects of truckloads.

The truckloads shown in Table 1 were considered in the analysis. Transverse distribution factors were calculated using both the lever rule and the equations provided in the AASHTO-LRFD specification (2017). Ultimately, a transverse distribution factor of 0.8908 lanes per stringer was determined to be critical, which was based on the lever rule with two lanes loaded. Using this distribution factor, truck loads were applied to the influence lines by moving the load pattern in 1' intervals over the entire 800' length of the bridge both forwards and backwards. Where variable axle spacings were called for, they were varied at 2' intervals. Individual axle loads that acted to mitigate the overall moment were not included. Lane loads that were part of the truckload patterns were applied only to segments of the bridges where they contributed to the moments being considered. A dynamic load allowance of 33% was applied to the axle loads of all trucks but was not applied to lane loads. A load factor of 1.75 was used for truckloads when rating at the inventory level and a load factor of 1.35 was used for truckloads when rating at the operating level. When rating for emergency vehicles, a distribution factor of 0.6345 lanes per stringer was used, which was based on one lane loaded without multiple presence. A load factor of 1.30 was used for rating emergency vehicles at both the inventory and operating levels.

Table 1: Truck Configurations Considered During 1DBL Analyses and Rating

HL-93 Design Loads	AASHTO Loads	Special Hauling Vehicles
• Truck + Lane	• Type 3	• SU4 • SU5
• Tandem + Lane	• Type 3S2	• SU6 • SU7
• Two Trucks + Lane	• Type 3-3	
	• $2_{\times}$ Type 3-3 + Lane	

Ohio Legal Loads	Emergency Vehicles	Notional Rating Load
• 2F1 • 3F1	• EV2 • EV3	• NRL
• 4F1 • 5C1		

The moment capacity that was used for rating purposes was based on Appendix A6 of the AASHTO-LRFD specification (2017). The top flanges of the stringers are continuously laterally supported by the concrete deck and haunches while the bottom flanges are laterally supported at 25'-0" intervals at their connections to the floor beams. Yielding / plastic hinging was the critical mode of failure in positive moment regions while lateral-torsional buckling (LTB) was the critical mode of failure in negative moment regions. The strength model used for plastic hinging is well established and is taken as the product of the plastic section modulus and the yield strength of the steel. The strength model used for LTB is based on an eigensolution of the buckling problem and includes a moment gradient modifier, C_b, to account for non-uniform distributions of moment over the unbraced length.

Moment Gradient Modifier:

Lateral-torsional buckling occurs when the compression flange of a member subjected to bending wants to buckle, but is restrained by the tension flange. If the compression flange is not adequately braced against lateral displacement and/or torsion, it can create lateral and torsional global buckling of the member. The design equations for lateral-torsional buckling in AISC 360-16 and Appendix A6 of the AASHTO LRFD Specification (2017) were developed based on beam-theory for the elastic torsional buckling of a doubly-symmetric I-section with uniform major-axis bending (Timoshenko and Gere, 1961). In order to incorporate moment gradient effects in the flexural capacity of a bending member, numerical or approximate solutions are needed. The moment gradient modifier, C_b, can be used to provide a simplified method of accounting for moment gradients across the unbraced length of the member while still using the design equations for uniform bending.

Beams subjected to gravity loading (with compression in the top flange) are often laterally braced against lateral-torsional buckling by a concrete slab. Continuous lateral bracing is typically achieved by connecting the top flange of the beam to the slab with shear studs. The Combs-Hehl stringers are not positively connected to the slab using shear studs, however; instead, the slab is haunched around the top flange of the stringers, as shown in Figure 1. It is reasonable to assume that the haunched slab will laterally brace the top flange of the stringer across its full length. Thus, lateral-torsional buckling will not occur when the top flange of the beam is in compression, but it

must be evaluated when the bottom flange is in compression, which primarily occurs at the stringer supports when the continuous stringers experience negative moment. The possible methods for calculating C_b for this loading scenario are explained in this section.

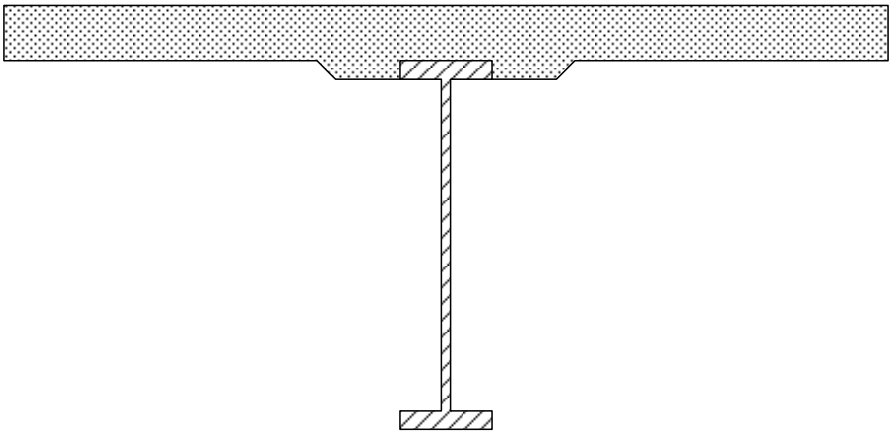

Figure 1: Haunch at Top Flange of Stringer

Article A6.3.3 of AASHTO (2017) uses a C_b value of 1.0 for unbraced cantilevers and members where $M_{mid}/M_2 > 1$ or $M_2 = 0$. M_{mid} and M_2 are the major-axis bending moments at the middle and end of the beam's unbraced length, respectively. Thus, if the moment at the midspan of the unbraced length is larger than the end moment (which is the case for many of the loading scenarios on the Combs-Hehl Bridge) or if either end moment is zero, $C_b = 1$ ought to be used. For all other cases, C_b is permitted in AASHTO Equation A6.3.3-7 to be calculated as:

$$C_b = 1.75 - 1.05\left(\frac{M_1}{M_2}\right) + 0.3\left(\frac{M_1}{M_2}\right)^2 \leq 2.3 \qquad \text{(Eqn 1)}$$

In Equation 1, M_1 is the intercept of the most critical assumed linear stress variation passing through M_2 and either M_{mid} or M_o, the brace point opposite location M_2. The application of this equation is shown graphically in Figure 2 using compressive stresses, f, in place of moments (AASHTO Article 6.10.8.2.3).

This approach generally provides accurate to conservative values for C_b but the AASHTO commentary notes that the refined AISC equation for C_b provides more accurate and less conservative results than what is proposed in AASHTO, particularly for cases where $M_{mid}/M_2 > 1$ or $M_2 = 0$. AASHTO references Galambos (1998), the 5th edition of the SSRC Guide, for other more refined calculations of C_b. Equation 1 was used in the AISC Specification from 1961 until it was replaced in 1986. AISC 360-16 promotes the formulation shown in Equation 2, which is a modification of work by Kirby and Nethercot (1979), for calculation of C_b:

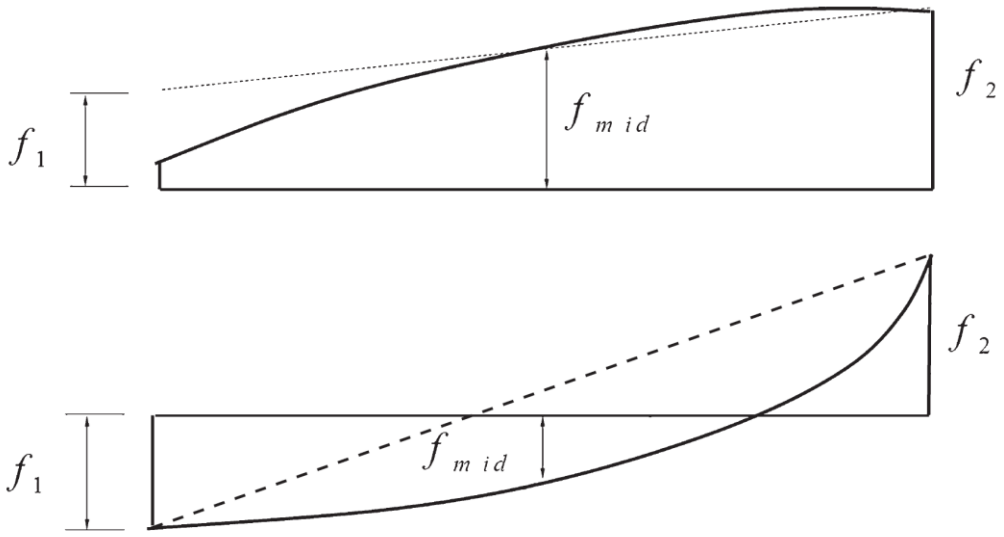

Figure 2: Application of AASHTO Moment Modifier Equation (Ziemian, 2010)

$$C_b = \frac{12.5M_{max}}{2.5M_{max} + 3M_A + 4M_B + 3M_C} \qquad \text{(Eqn 2)}$$

where M_{max} is the absolute value of the maximum moment in the unbraced segment and M_A, M_B, and M_C are the absolute values of the moments at the quarter, mid and three-quarter points, respectively. This equation was found to be accurate and conservative for most load cases (Wong and Driver, 2010). It also provides a more accurate solution than the AASHTO approach for unbraced lengths with nonlinear moment diagrams such as continuous beams with no lateral bracing within the span that is subjected to a uniformly distributed transverse load (the case for the stringers in the Combs-Hehl Bridge).

Yura and Helwig (1995, 2010) developed an expression for gravity loaded wide flange beams with the top flange laterally restrained that is provided in the commentary of the AISC Specification (AISC 360-16).

$$C_b = 3.0 - \frac{2}{3}\left(\frac{M_1}{M_0}\right) - \frac{8}{3}\left[\frac{M_{CL}}{\left(M_0 + M_1\right)^*}\right] \qquad \text{(Eqn 3)}$$

In Equation 3, M_0 is the moment causing the largest bottom flange compressive stress at the end of the unbraced length, M_1 is the moment at the other end of the segment, and M_{CL} is the moment at the middle of the unbraced length, as is shown in Figure 3. The equation works well for linear moment diagrams as well as nonlinear moments due to distributed loading. It is unconservative when the span-to-depth ratio of the beam is low (approximately 15) and the center moment and end moments are all negative. This occurs when significant loading at adjacent spans can cause the span to experience negative moment along its entire unbraced length, which occurred occasionally in the analysis of the Combs-Hehl Bridge. For these limited cases, the AISC approach

(Eqn. 2) for C_b was used; for all other loading scenarios, Yura and Helwig's equation (Eqn. 3) was used.

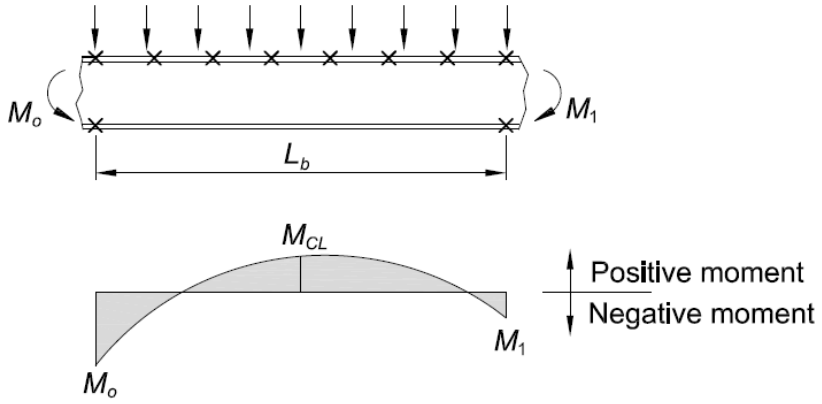

Figure 3: Yura and Helwig Approach to Moment Gradient

In many bridge analyses, the moment gradient modifiers are computed based on moment envelopes using non-concurrent moments. Using refined formulations for the moment gradient modifier, however, requires that C_b be calculated using concurrent moments from diagrams instead of envelopes (AASHTO 2017). As a result, a unique value of C_b was computed for every unbraced span, for every truck considered, and for every truck position considered. Thus for 16 spans, 59 truckload permutations, and approximately 800 truck positions, 755,200 unique values of C_b were computed for the 1DBL analyses. Considering that rating factors were computed at 12 points along each 25' long span, approximately 9,000,000 rating factors were computed for the 1DBL analyses. The governing rating factor for each class of truck loading is shown in Table 2. It was found that the HL-93 design loading resulted in the lowest stringer rating. Excluding the HL-93 design load, the Special Hauling Vehicle (SHV) SU7 was the critical truckload and resulted in the lowest rating when positioned with the front axle 12' from any of the interior floor-beam support locations.

Table 2: Rating Factors based on 1D Beam-Line Analysis Approach

	Operating	**Inventory**
HL-93 Design Loads:	RF = 1.11	RF = 0.86
AASHTO Rating Vehicles:	RF = 1.64	RF = 1.26
Notional Rating Load:	RF = 1.48	RF = 1.14
Special Hauling Vehicles:	RF = 1.48	RF = 1.14
Ohio Legal Loads:	RF = 1.67	RF = 1.29
Emergency Vehicles:	RF = 1.31	RF = 1.31

3D Linear Elastic Modeling

Three dimensional linear-elastic (3DLE) finite element models of the bridges were created using the SAP2000 software. The models included main girders, floor beams, and stringers, all modeled using beam elements, as well as the deck, which was modeled using shell elements. The weight of the barrier walls was included in the model but the barrier stiffness was not included. The girders were supported at the pier locations every 200'. Modeling efforts focused on the south bridge but results were corroborated using a model of the north bridge. A view of the unloaded model with the deck elements hidden is shown in Figure 4.

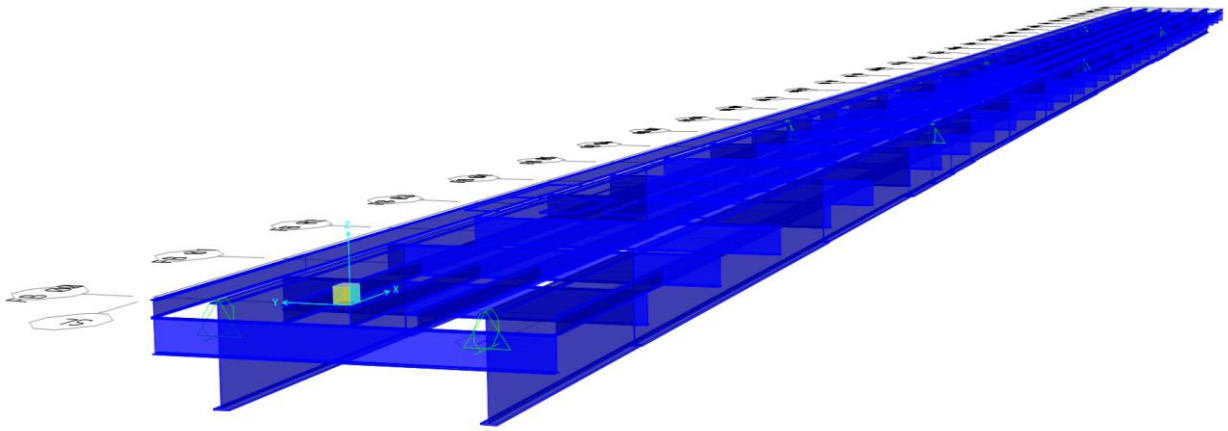

Figure 4: 3D Linear Elastic Model of the South Bridge

The model was loaded with two SHV SU7 trucks spaced side-by-side straddling Stringer J, adhering to the lane definitions in the AASHTO-LRFD specification (2017). The longitudinal position of the trucks was varied by moving the trucks at 1' increments over the length of the bridge both forwards and backwards. A view of the deflected model with the trucks positioned near the middle of Span 7 with the front axles of the trucks positioned 87' east of Pier 6 is shown in Figure 5, where the deflection has been amplified by a factor of approximately 12 for clarity.

Strength calculations used to rate the stringers in the 3DLE analyses were identical to those used with the 1DBL ratings. The critical results of the analyses and rating are shown in Table 3, which is based on C_b values computed using the modified Yura and Helwig approach described earlier. Table 4 shows the same critical results calculated using C_b =1.0. The stations that are referenced in these tables are measured eastwards from Pier 6. Station 72' represents the critical positive-moment rating in the stringer, Station 200' represents the critical negative-moment rating in the stringer, and Station 10' represents the critical positive-moment rating in the end stringer span, which employed heavier stringer sections.

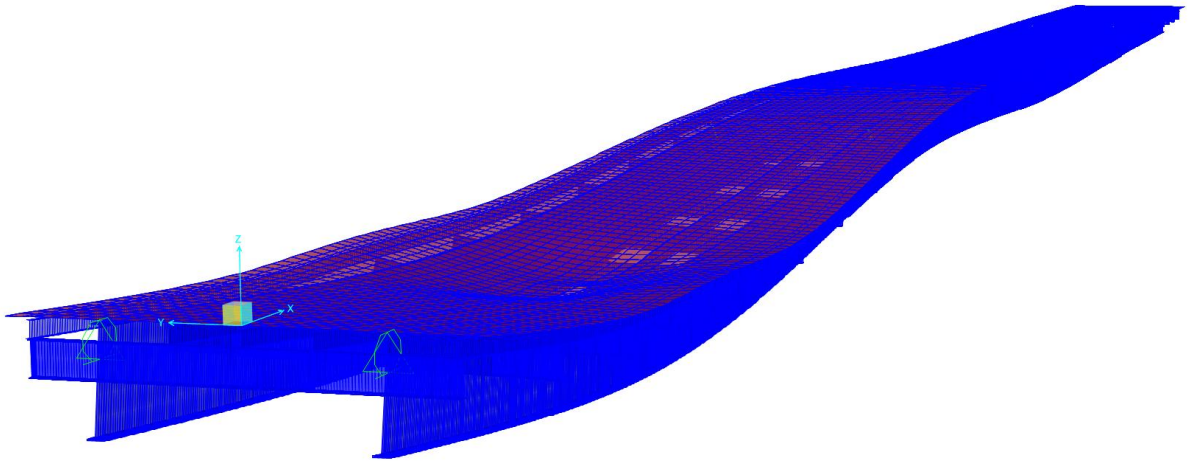

Figure 5: Deflected Shape of the 3D Linear Elastic Model with Truck Loads in Span 7

Table 3: Critical Rating Factors Based on 3DLE Analyses with Helwig C_b

	Operating	**Inventory**
Station 72':	RF = 3.88	RF = 2.99
Station 200':	RF = 6.22	RF = 4.80
Station 10':	RF = 4.40	RF = 3.39

Table 4: Critical Rating Factors Based on 3DLE Analyses with C_b = 1.00

	Operating	**Inventory**
Station 72':	RF = 1.48	RF = 1.14
Station 200':	RF = 1.49	RF = 1.15
Station 10':	RF = 1.61	RF = 1.25

It is postulated that the less conservative rating factors that were calculated using the 3DLE method are reflective of the three-dimensional behavior of the bridge that is captured in the 3DLE analyses but not in the 1DBL analyses. In the 1DBL analyses, the stringers are supported at 25' 0" intervals by supports that are infinitely rigid vertically. In the 3DLE analyses, however, the stringers are instead supported by floor beams that deflect vertically as the supporting girders deflect. The girders, with their spans of 200', are the primary load carrying elements in bridge and their deflection affects the load distribution within the stringers in a way that reduces the moment demand on the stringers.

3D Nonlinear Inelastic Modeling

Three dimensional nonlinear-inelastic (3DNI) finite element models of the bridges were created using the ABAQUS software. The models included the main girders, floor beams, stringers and deck, all modeled using shell elements. Transverse members between the stringers at the floor beam locations were not included in the model; their presence would likely have increased the strength of the stringers. The weight of the barrier walls was included in the model but the barrier stiffness was not included. The girders were supported every 200' at the pier locations. Modeling efforts focused on the south bridge but results were corroborated using a model of the north bridge. Because of the rigor of analyzing the 3DNI models, most analyses were performed on 200' long or 400' long segments of the bridges, often spans 7 and 8. A view of the unloaded 3DNI model of the south bridge with the deck elements hidden is shown in Figure 6 and a view of the unloaded 3DNI model of the north bridge with the deck elements hidden is shown in Figure 7.

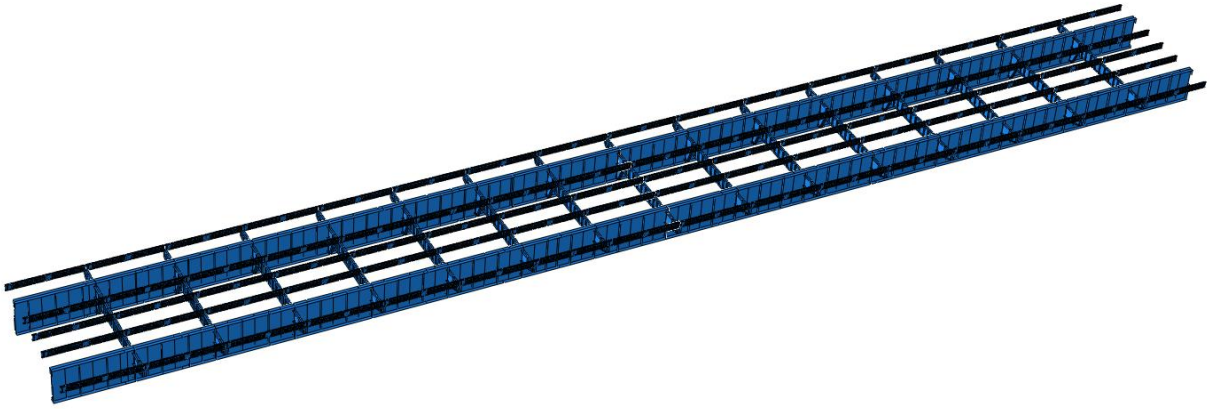

Figure 6: View of the 3DNI Model of the South Bridge

The goal of the 3DNI modeling was to confirm results from the 3DLE analyses and ratings for critical truck configurations and positions. Because the 3DNI models were used for both the determination of the moments in the stringers and for determination of the stringer strengths, they were naturally far more detailed than the 3DLE models. The 3DNI models were based on shell elements and included details such as residual stresses and initial geometric imperfections that were necessary to capture buckling failures effectively. Additionally, contact and separation behavior was defined between the deck and top flanges of the stringers and analytical constraints were defined to represent connections between the stringers and floor beams and between the floor beams and main girders.

Standard S4R shell elements with four nodes, hourglass control, reduced integration, and finite membrane strains were used throughout the models. Web elements were defined at mid-thickness of the web while flange elements were defined at outside surfaces of flanges in order to maintain consistency of the overall depth of the members in the model with the actual depth of the sections. Stiffeners were modeled explicitly. All steel was defined as elastic perfectly plastic using A36

properties with F_y = 36[ksi], E = 29,000[ksi], and ν = 0.30. Concrete was defined with f'_c = 4,000[psi] using nonlinear behavior based on the "Concrete Damaged Plasticity" material model in ABAQUS, though no inelastic behavior was observed in the concrete in any of the analyses. The mesh size for stringers is determined by the breadth of the strips used to assign the residual stresses, 0.87625" wide in the flange and 1.475" in the web. The length of the elements is 1.5", resulting in elements that have appropriate aspect ratios. Meshing of a typical stringer is illustrated in Figure 8.

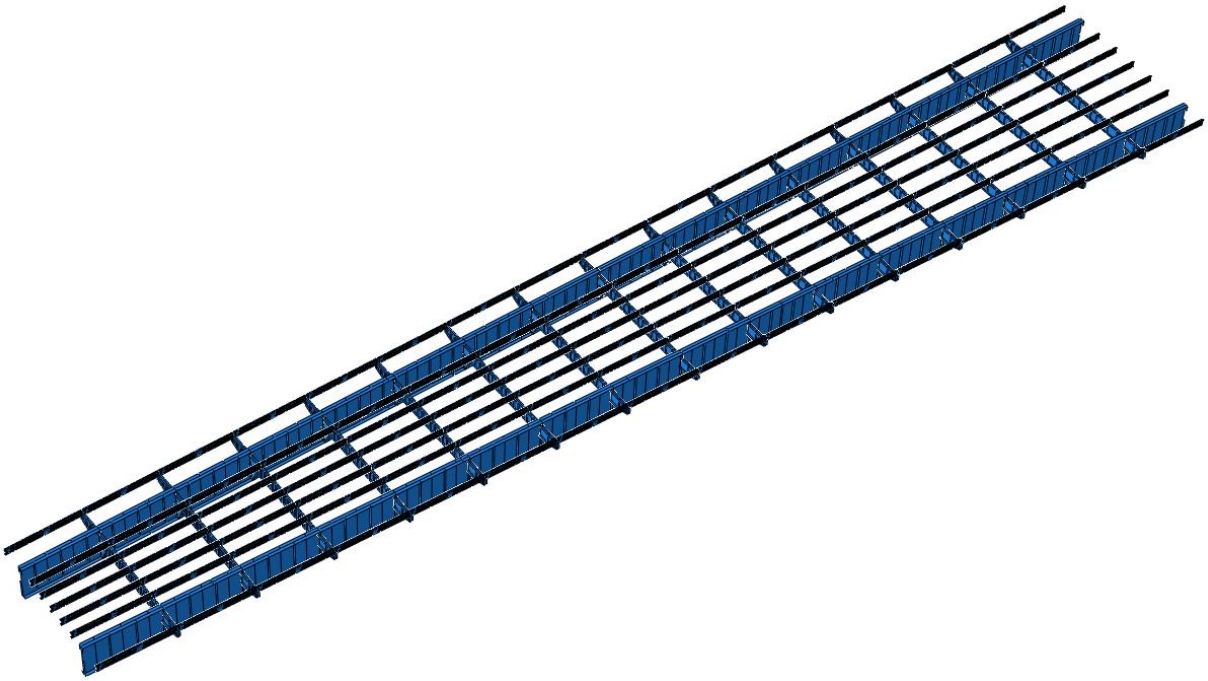

Figure 7: View of the 3DNI Model of the North Bridge

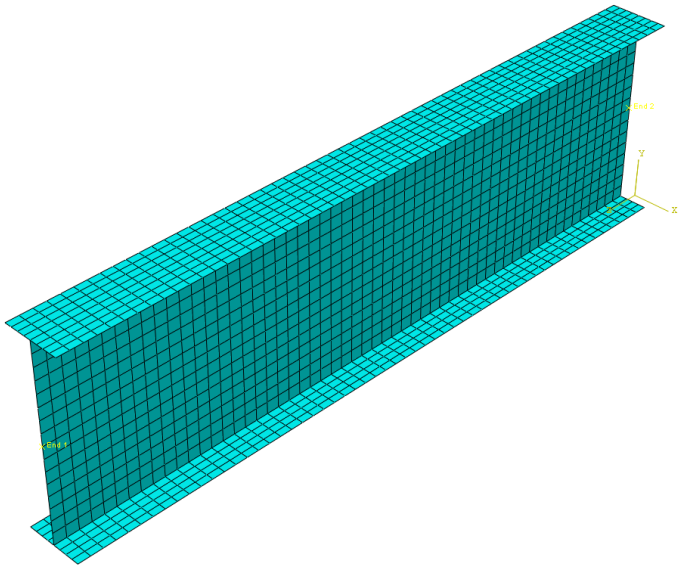

Figure 8: Meshing of a Typical Stringer in the 3DNI Models

Residual strains were included in the model using predefined fields for direct specification of the stress values. The flanges were divided into eight strips of even breadth, while the web was divided into 16 even strips. The values of the residual stresses applied to these strips were determined using the distribution of residual stress suggested by Szalai and Papp (2005). The average value of stress over the breadth of the strip was applied to the whole strip.

Geometric imperfections were included as the genesis of local buckling and lateral buckling modes of failure and were defined by superimposing vibrational mode shapes. With the exception of the beams of 5'-6" in length and shorter, initial imperfections were included at a magnitude of (1"/80')×(length) based on three buckling modes including (i) weak direction buckling, (ii) torsional buckling, and (iii) a mode including both flange and web local buckling. Beams of 5'-6" in length and shorter included only the first mode, as the localized modes were unlikely to activate. Weak direction buckling and torsional buckling were applied such that the displacements were in the same direction for the flange that was expected to be in compression.

The concrete deck and haunches of Combs-Hehl approach spans embed the top and sides of the top flanges of the stringers, though there are no studs to ensure composite behavior. This concrete prevents the flange from moving into the concrete, though not away from it; thus, the top flange may buckle downward but not upward. Flanges are compact, so flange local buckling was not likely, but these limits were included nonetheless using analytical constraints in ABAQUS called "connectors." These connectors are defined along the local Cartesian axes of the elements and prevent the steel from penetrating the concrete, but do not prevent the steel from separating from the concrete. Normal behavior is "hard" and allows separation following contact while tangential behavior was imposed with penalty functions using a coefficient of friction, $\mu = 0.20$.

Validation of Modeling Approach:

The performance of the 3DNI models was validated by comparing results of a model of a single stringer to the theoretical moment capacity of the section as determined by the equations in AASHTO for plastic moment and lateral-torsional buckling over a varying range of unbraced lengths. The theoretical results based on a uniform moment ($C_b = 1.00$) are shown as a solid line in Figure 9 while the 3DNI model results obtained without lateral support of the deck are shown as circles. The 3DNI model matches the theoretical equation well in the plastic moment capacity and the nonlinear region of LTB, while slightly overestimating the capacity in the linear buckling region somewhat at unbraced lengths beyond approximately 200". This is not unexpected, however, as the theoretical models were developed as lower bound curves to be applied to any beam-type cross section, while the model results are specific to the sections being modeled. The model results lack the kink visible in the theoretical solution where the plastic moment capacity transitions to inelastic LTB, likely because the initial geometric imperfections used in the model were not random but were instead based on the lower buckling modes, which predisposes the models to buckle in modes similar to those.

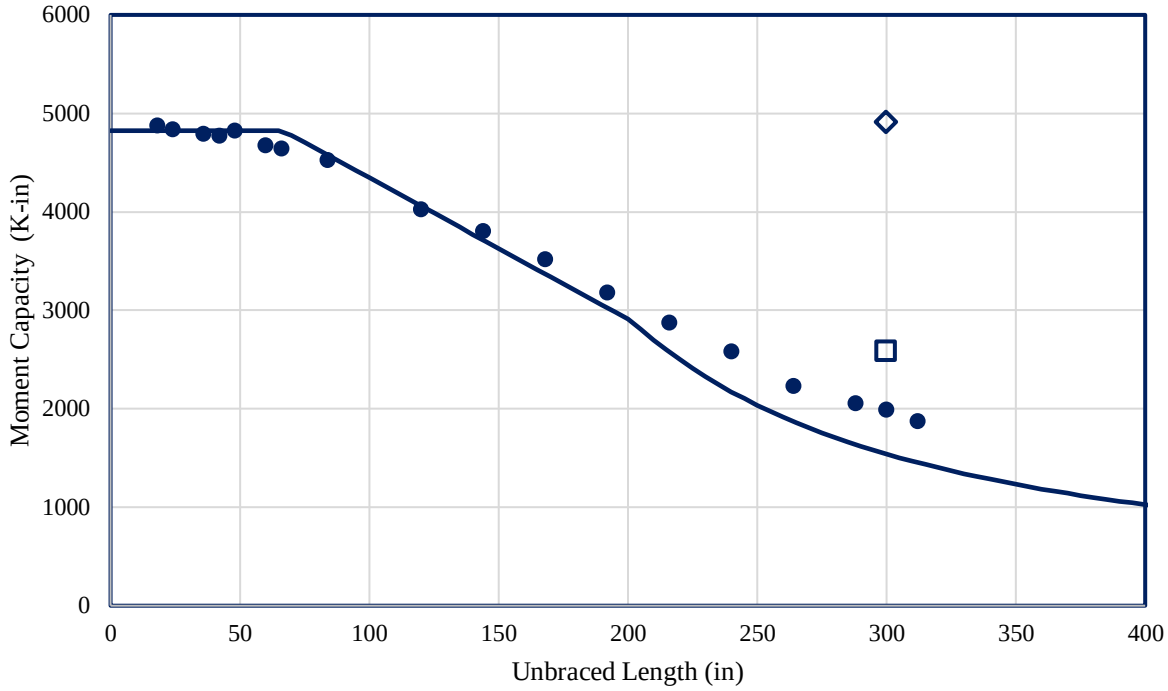

Figure 9: 3DNI Model Validation for a W24×55 Stringer with A36 Material

To validate the model for loadings other than a uniform moment, a model of an unbraced beam with an unbraced length of 25'-0" = 300" was subjected to a mid-span point load. This result, which includes the appropriate moment gradient modifier, is shown in Figure 9 as a square and matches theoretical strength well. The diamond shown in Figure 9 represents the strength of the stringer predicted by the model when the lateral restraint provided by the deck and haunches is included. It matches well with the theoretical plastic moment strength of the section.

Bridge Modeling and Rating:

Since the models of the approach spans include girders, floor beams, and stringers all modeled using shell elements, additional analytical constraints were defined to represent the connections in the actual bridge. Each stringer has a small region (6" long) on the bottom of the flange that is analytically tied to the top flange of the supporting floor beam, restricting displacement and rotation of the stringers' bottom flanges. A typical stinger-to-floor beam connection in the 3DNI model is shown in Figure 10 where defined contact interactions between the stringer and floor beam are shown as circles. Defined contact interactions between the deck and top stringer flange are shown as squares. Each floor beam is connected analytically to the two girders using tie constraints in four places; on the inside and outside faces of each of the two girders.

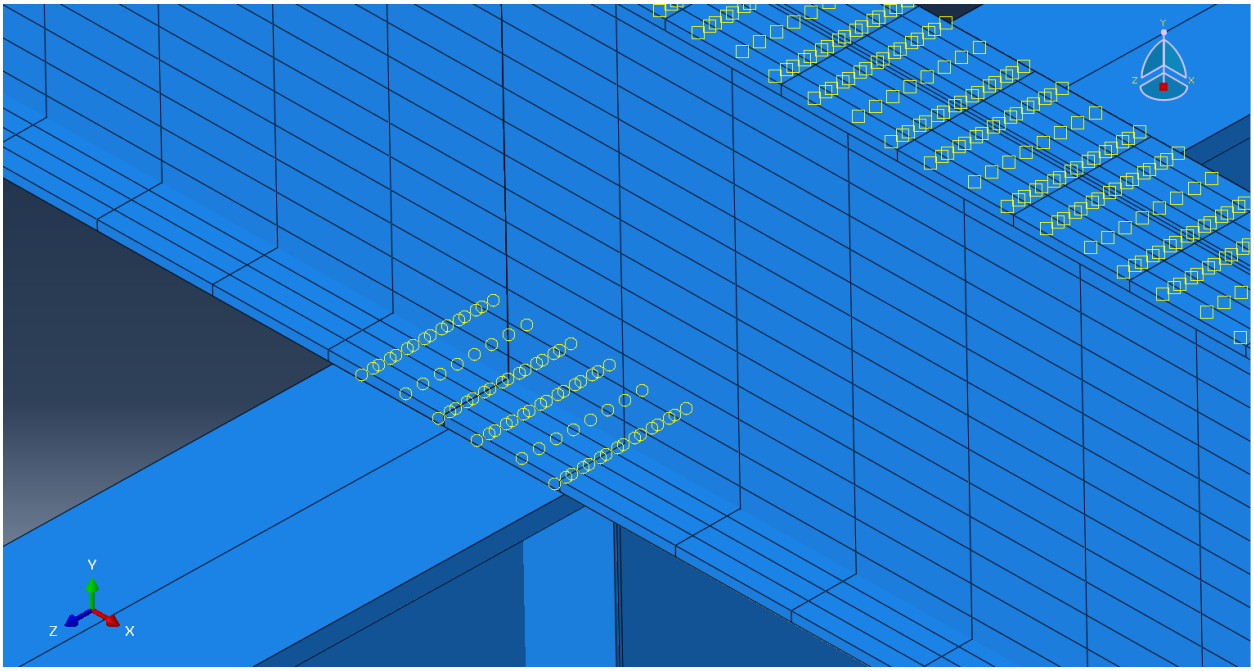

Figure 10: Stringer Contact Interactions in the 3DNI Model

The 3DNI bridge models were loaded using uniform pressures for permanent loads other than self-weight, all including appropriate load factors, and point loads representing the wheel loads, as is shown in Figure 11. The magnitude of the truckloads was then incrementally increased until a failure in the model was observed as an analytical instability (failure of the analysis to converge to a solution during a given increment). The magnitude of the truckloads at failure divided by the nominal weight of the trucks is defined as the truckload factor, *TLF*. For example, two SHV SU-7 Trucks causing a failure in the model with *TLF* = 1.6 would indicate a failure due to two trucks each with a total weight of $1.6 \times 77.5^{kip} = 124.0^{kip}$. This truck load factor, *TLF*, should not to be confused with the load factors, γ, that are used in design and rating using the 1DBL and 3DLE methods. The rating factor is then obtained by,

$$RF = \frac{TLF}{(LL + IM) \times \gamma_{LL} \times MPF} \qquad \text{(Eqn 4)}$$

where *IM* is the impact factor, γ_{LL} is the AASHTO defined load factor for live loads, and *MPF* is the appropriate AASHTO multiple presence factor for the loading used.

Based on 1DBL and 3DLE analyses and ratings, the truck loads that were evaluated using the 3DNI analyses consisted of two loading scenarios: (1) two SHV SU-7 trucks side-by-side positioned over Pier 7 (front axles located at Station 209' relative to Pier 6), which was the critical position for negative moment in the stringers over the floor beams, and (2) two SHV SU-7 trucks side-by-side positioned near the middle of Span 7 with the front axles of the trucks near Station 87' relative of Pier 6, which was the critical position for positive moment in the stringers. Negative moment proved to be critical and those results are described here.

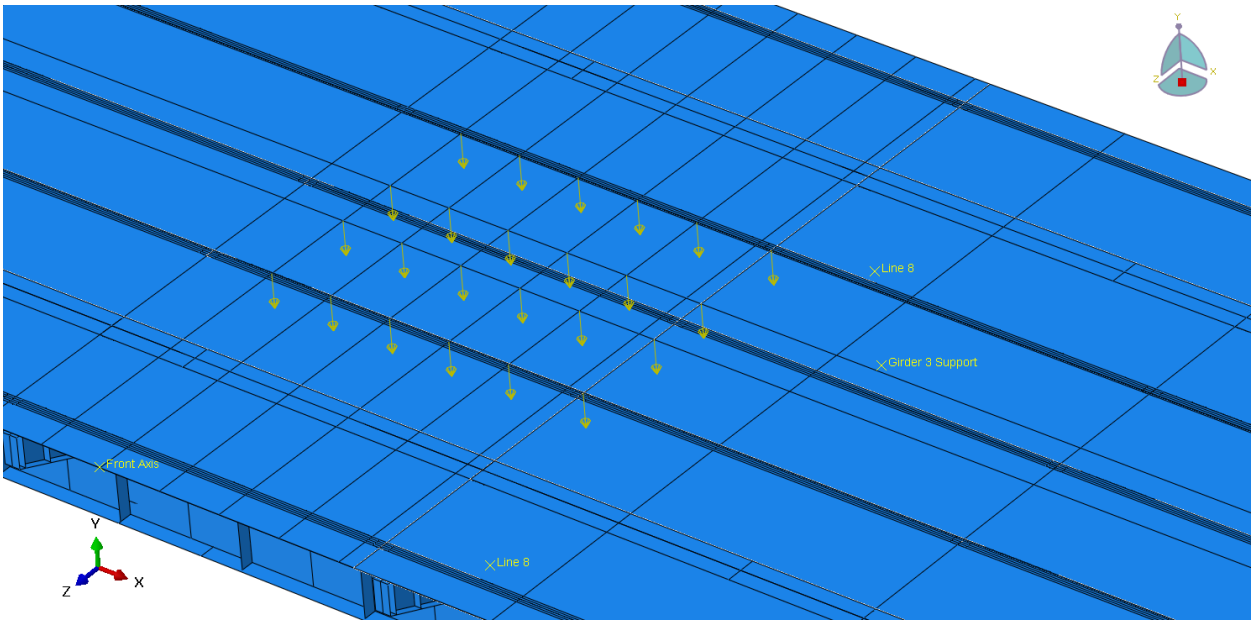

Figure 11: Truck Load Application to the Deck of a 3DNI Model

The models were initially analyzed with nonlinear material properties for all steel and concrete. The first analysis resulted in an observed failure in the main girders. Since the girders were not the focus of the study, however, the girder elements were redefined with elastic material properties to preclude girder yielding and the model was analyzed again. The second analysis resulted in an observed failure in Floor Beam #8, as shown in Figure 12. Since the floor beams were not the focus of the study, the floor beam elements were redefined with elastic material properties to preclude yielding of these elements, and the model was analyzed a third time. The third analysis resulted in an observed failure in the stringers near Floor Beam 8, over Pier 7, as is illustrated in Figure 13.

The Truck Load Factor, *TLF*, was plotted as a function of stringer deflection for this analysis and is shown in Figure 14, where the curved bold line representing the nonlinear stringer response is plotted against a straight line for reference. It can be observed that the stringer response was approximately linear until a live load approximately equal to six times the weight of two SHV SU-7 trucks was applied ($TLF \leq 6$). The analysis reached an analytical instability and stopped when a live load approximately equal to ten times the weight of two SHV SU-7 trucks was applied ($TLF = 10$).

For rating at the operating level, if failure is based on the first observance of yielding / nonlinear behavior in the stringer, then the rating factor can be estimated as,

$$RF = \frac{6.0}{(1.33)\times(1.35)\times(1.00)} = 3.34 \qquad \text{(Eqn 5)}$$

The corresponding rating factor at the inventory level based on first yielding would be $RF = 2.58$.

Alternatively, for rating at the operating level, if failure is based on the development of an instability in the stringer, then the rating factor can be estimated as,

$$RF = \frac{10}{(1.33)\times(1.35)\times(1.00)} = 5.57 \qquad \text{(Eqn 6)}$$

The corresponding rating factor at the inventory level based on an instability would be RF = 4.30.

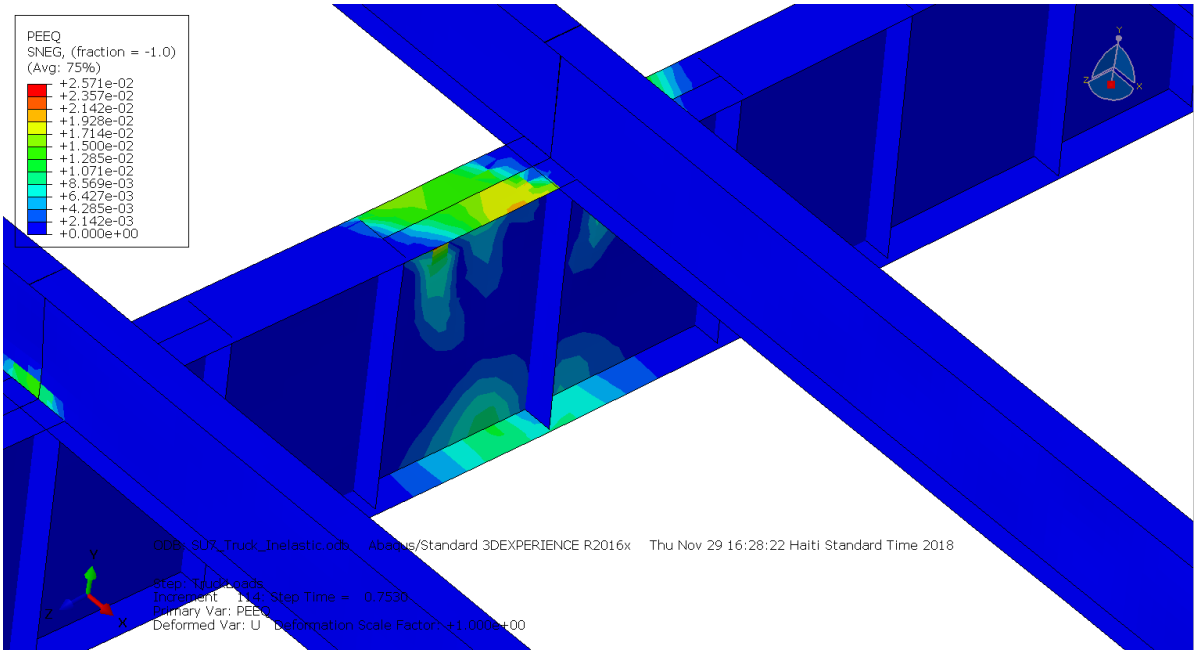

Figure 12: Stress Contour Illustrating Failure of Floor Beam #8

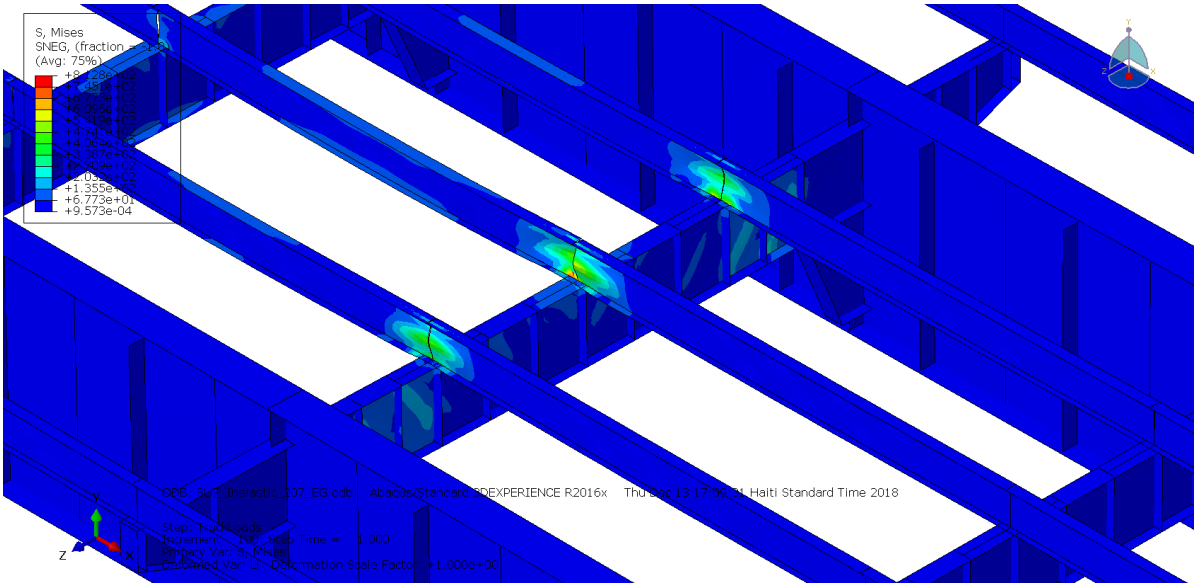

Figure 13: Stress Contour Illustrating Failure of Stringers I, J, and K

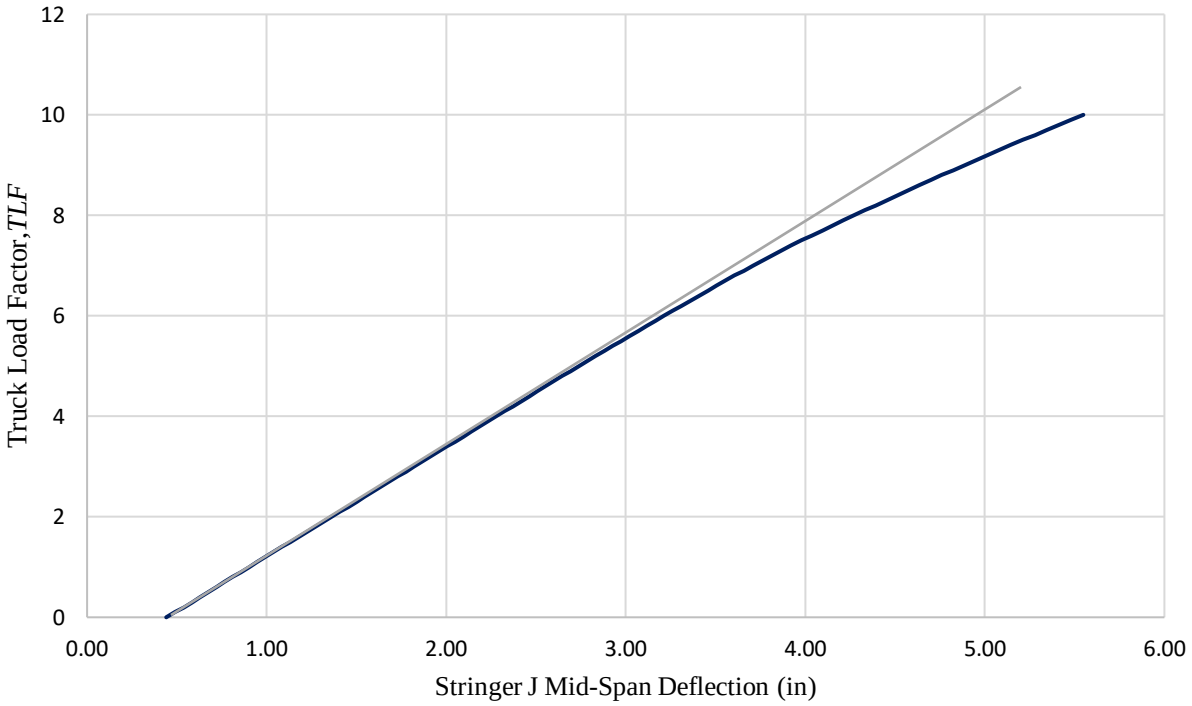

Figure 14: Truck Load Factor vs. Stringer Deflection for Critical 3DNI Stringer Analysis

Stringer Web Strength:

At the request of the ODOT advisory panel, the web crippling and web yielding strengths of the stringers were evaluated. Stringers near the end of the approach spans at Pier 6 were selected as critical based on professional judgement. At that location, the stringer sections are W24×76 (A36). Using the AASHTO LRFD provisions (2017), the web yielding strength was found to be $\phi R_n = 205^{kip}$ and the web crippling strength was found to be $\phi R_n = 139^{kip}$. Demand at that location was determined using the 3DLE model and was found to be 2.8^{kip} due to *DC* + *P* loads and 6.4^{kip} due to *LL* + *IM* loads when subjected to the SHV SU-7 truck loading. Based on this, the rating factor for the web crippling was found to be approximately equal to 11 at the inventory level.

Conclusions:

Based on the 1D Beam Line analysis and rating, the minimum operating rating factor for the stringers was found to be 1.11 due to the HL-93 design loads. The next smallest operating rating factor was found to be 1.31 due to Emergency Vehicle Loading (one lane loaded using a multiple presence factor of 1.20). Finally, the next smallest operating rating factor was found to be 1.48 due to the Special Hauling Vehicle SU7. Based on the 3D Linear Elastic modeling and rating, the

minimum operating rating factor due to the SHV SU7 truck loading was found to be 3.88. Based on the 3D Nonlinear Inelastic modeling and rating, the minimum operating rating factor due to the SHV SU7 truck loading was found to be approximately 5.57 based on an instability in the stringers . These results are summarized in Table 5.

Table 5: Rating Factors for SHV SU7 Based on Different Methods of Analysis and Rating

	Operating
1D Beam Line:	RF = 1.48
3D Linear Elastic:	RF = 3.88
3D Nonlinear Inelastic:	RF = 5.57

References:

AASHTO (2018), AASHTO Manual for Bridge Evaluation, 3rd Edition, American Association of State Highway and Transportation Officials, Washington DC, Sep 2018

AASHTO (2017), AASHTO LRFD Bridge Design Specifications, 8th Edition, American Association of State Highway and Transportation Officials, Washington DC, Sep 2017

AISC 360-16 (2016), Specification for Structural Steel Buildings, American Institute of Steel Construction, Chicago, IL, July 7, 2016

Galambos, T. V. (1998), Guide to Stability Design Criteria for Metal Structures, Fifth Edition, Structural Stability Research Council, John Wiley and Sons, Inc., New York, NY.

Kirby, P.A. and Nethercot, D.A. (1979), Design for Structural Stability, John Wiley & Sons Inc., New York, NY.

Szalai, J., and Papp, F. (2005). "On the Probabilistic Evaluation of the Stability Resistance of Steel Columns and Beams," Journal of Constructional Steel Research 65, no. 3 (2009): 569-577.

Timoshenko, S. P., and Gere, J. M., (1961) Theory of Elastic Stability, McGraw-Hill, New York.

Wong, E. and Driver, R. G. (2010), "Critical Evaluation of Equivalent Moment Factor Procedures for Laterally Unsupported Beams," Engineering Journal, AISC, Vol. 47, No. 1.

Yura, J.A. (1995), "Bracing for Stability - State-of-the-Art," Proceedings of the ASCE Structures Congress XIII, Boston, MA, ASCE, New York, NY, pp. 88–103.

Yura, J.A. and Helwig, T.A. (2010), "Buckling of Beams with Inflection Points," Proceedings, Annual Stability Conference, Orlando, FL, North American Steel Construction Conference, SSRC.

Ziemian, R. D. (2010), Guide to Stability Design Criteria for Metal Structures, Sixth Edition, Structural Stability Research Council, John Wiley and Sons, Inc., New York, NY.